Semi-Autonomous Bulldozer Blade Control Using Real-Time Terrain Mapping

Teemu Mononen, Antti Kolu, and Jouni Mattila

***Abstract*— This paper considers semi-autonomous excavation done by heavy-duty bulldozers with an onboard front-mounted blade. The goal is to gradually manipulate the blade digging depth to maximize the amount of excavated soil while considering the approaching terrain shape, traction, and the mobile base inclination. With the proposed system, the operator provides the target load on the machine and the blade is controlled semi-autonomously, while the operator can focus on driving the mobile base. To reduce large load variations caused by terrain shape irregularities affecting the blade, our system uses an onboard lidar to generate an elevation map of the terrain, updating it online as the machine moves. From the discrete map, we generate a well-behaved function describing the terrain shape. This provides a nominal blade elevation path that is modified online based on the measured load on the machine to maneuver the blade gradually, avoiding large gradient changes. The resulting Cartesian elevation profile is used as a reference to a blade position controller that counteracts the mobile base inclination. A commercial bulldozer with no modifications to its original hydraulics was used as an experimental platform, and the results verify the efficacy of the proposed methods in challenging outdoor conditions.**

I. Introduction

The bulldozer is a mobile heavy-duty earthmoving machine used for cutting and pushing soil material with an onboard blade. Typically, bulldozer operators move soil material by manipulating the blade digging depth based on a number of factors. An experienced operator aims to move as much material as possible while monitoring the machine's *tractive performance*, *approaching terrain*, and *the mobile base inclination*. They maneuver the blade gradually to create a smooth profile for the tracks to drive on, as it is difficult to maintain a full blade when the mobile base inclines on uneven terrain. Automatically controlling the blade elevation reduces the workload of an operator and can increase the productivity by maintaining a desired load on the machine. However, when there are slopes or gradient changes in the existing terrain, the performance of an automatic blade control system degrades if this information is not included to the automatic system. If such systems only react to measurements of the machine state, positive gradients in the terrain cause unexpected track slip and negative ones cause loss of material off the blade. Hence, the performance of automatic blade load control systems can be increased by sensing the terrain shape and using that information in the control loop [1]. That way, an automatic blade controller can react to ground profile variations before they affect the load on the machine. The controller can then consider the same quantities as an experienced operator to decide the elevation followed by the blade cut edge.

The two typical *traction control* strategies for mobile earthmoving machines are wheel torque control and implement depth adjustments [2]. While the latter method can be applied on machines with rear-mounted implements without posing constraints on the resulting surface shape [3], the bulldozer's implement is positioned in the front, making the implement locus determine the mobile base inclination in the near future. It is desirable to control the blade to generate a profile with small gradient changes for the tracks to drive on. This improves travel comfort, maximizes the track surface area against soil, and reduces correcting motions required from the blade. The latter is important in automatic control of systems with proportional hydraulic valves designed for manual operation. In that case, noticeable gradient changes in the terrain under the tracks can cause Cartesian position control errors, and wavy patterns in the resulting surface. Semi-automatic earthmoving by a commercial bulldozer was developed in [4], where the blade elevation was controlled based on the load experienced by the machine. Simulation results were presented in [5] for a bulldozer operating on uneven terrain without terrain shape information.

Terrain sensing by cameras and lasers has been applied in many academic works considering soil excavation [6, 7, 8, 9]. It is also possible to gauge the terrain by driving over it and recording the mobile base footprint. This was done with a bulldozer in [1] to then use the estimated terrain shape in control of the blade when the same area was excavated in the next pass. This solution does not have the terrain information available for the first pass and is not applicable in all work conditions (such as material spreading, where the soil to be spread cannot be traversed beforehand). To eliminate these problems, we apply visual sensing of the terrain by onboard sensors. A robust method for worksite mapping is required for mobile earthmoving machines that are subjected to vibrations and external acceleration caused by interactions with soil. A method robust to calibration and localization errors, and external disturbances was reported in [10], which based itself on [11]. Using a Bayesian update scheme accounting for different sources of uncertainty, the proposed algorithm showed promising accuracy when used on a hydraulic mobile work machine and is hence applied in this paper as well. Such an algorithm is computationally inexpensive, but the output cannot be directly used as an input to a control system. In [12], the blade reference for a scaled-down bulldozer was generated by a model predictive controller that aimed to maximize the material removal rate. The soil topography was obtained by a line laser, but the sensor was not installed onboard the mobile robot [13]. In [7], an onboard RGB-D camera was used on a laboratory bulldozer to determine the shape of a soil pile. A modified A*

Teemu Mononen and Jouni Mattila are with the Faculty of Engineering and Natural Sciences of Tampere University, Tampere, Finland. Direct all correspondence to teemu.mononen@tuni.fi.

Antti Kolu is with Novatron Oy, Tampere, Finland.

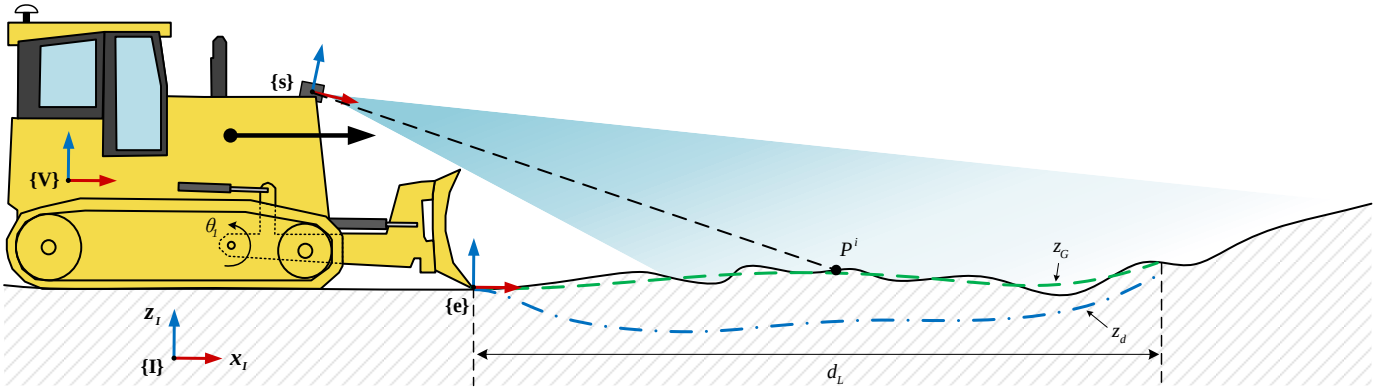

Fig. 1. The overall concept and coordinate frames of the design for worksite mapping and blade control. The resulting blade locus is shown as the blue dash-dot line that is computed online as explained in Section IV. The proposed localization algorithm estimates the relation between the vehicle frame **V** and the inertial frame **I**. The mapping algorithm uses points P^i from the point cloud measured by a lidar sensor to update the map.

algorithm was used to plan sequential pushes to move the soil pile to a predetermined dumping area. The authors tested the system in simulation and a scaled-down laboratory setup, where soil removal was done by mobile base motion as the blade elevation was not actuated.

Automatic grading systems offload the *mobile base inclination* compensation from the operator by automatically keeping the blade on target elevation. Blade position control to follow a predetermined site model has been considered for heavy-duty bulldozers in few academic publications [14, 15, 16] and commercialized by some machine manufacturers (e.g., [1]) and other companies (e.g., [17]). To the best of the author's knowledge, academic works considering the tractive performance in blade control are not widely available. In academic publications, lidar-based environment sensing has been implemented on heavy-duty bulldozers [18], but not as part of automatic control systems in full-size experiments.

In this paper, we present a semi-autonomous blade control scheme for bulk earthmoving implemented on a full-size commercial bulldozer with retrofitted sensors and no modifications to its original hydraulics. To retain the controller performance in different environmental conditions, we include estimation of the surrounding terrain topography using onboard sensors. The proposed blade controller can then consider similar quantities as an expert operator: the tractive capability is considered by load force feedback; the approaching terrain with real-time mapping and reference extraction; and the mobile base inclination by a blade position controller. Furthermore, these constraints are considered while maneuvering the blade smoothly. The blade control algorithm uses a well-behaved nominal path extracted from an online-updated discrete terrain elevation map and applies gradual elevation changes based on the deviation from the desired tractive performance. To this end, the measured load on the machine is filtered adaptively to reduce the impact of dynamic effects on the blade locus. The human operator provides the reference load on the machine and drives the mobile base. Experimental results on undulating terrain demonstrate that desired tractive performance is reached while cutting a smooth ground profile with the blade. Challenges to testing were caused by partially frozen ground, but the tests showcased that the proposed system functioned as intended when the machine was operated on manipulable soil.

The rest of the paper is organized as follows. In Section II, the studied problem and solution are introduced. Sections III and IV detail the used methods, with Section III describing terrain shape estimation, and Section IV blade control. The experimental setup is described in Section V, and experimental results are presented in Section VI. Finally, Section VII concludes the present study.

II. Problem Definition

In this paper, we consider semi-autonomous bulldozer blade control during the typical work cycle of excavating soil material. Such a work cycle consists of four subtasks: 1) loading the blade, 2) carrying the soil material on the blade, 3) unloading the material off the blade, and 4) reversing to next loading location. Here, we consider subtasks 1 and 2. The goal of the loading subtask is to accumulate a soil pile on the blade by lowering the end-effector frame below the ground as the machine moves forward in a straight line. In the carrying subtask, the blade is smoothly maneuvered to move the accumulated pile to an unloading area, where the unloading subtask would take place. The objective of this use case is two-fold: (i) move a full blade of material during each cycle, and (ii) achieve (i) by maneuvering the blade in a smooth way. In addition to the reasons described in Section I, smoothness is desired to have a suitable input for the control system, reduce unnecessary valve inputs, and to have the system react according to the expected tolerances of the outcome.

The overall solution concept is illustrated in Fig. 1. The terrain shape estimation relies on sensor data P^i from a lidar in frame $\boldsymbol{s}$ to generate a global elevation map of the environment. Then, using the map, a nominal path z_G describing the environment shape in the direction of motion is generated. This gives the blade controller the ability to consider the terrain shape as a feedforward term when computing the actual blade reference z_d. The nominal reference is computed up to distance d_L ahead of the end-effector frame $\boldsymbol{e}$, but the actual reference is only computed to the coordinates of frame $\boldsymbol{e}$ based on the measured tractive performance.

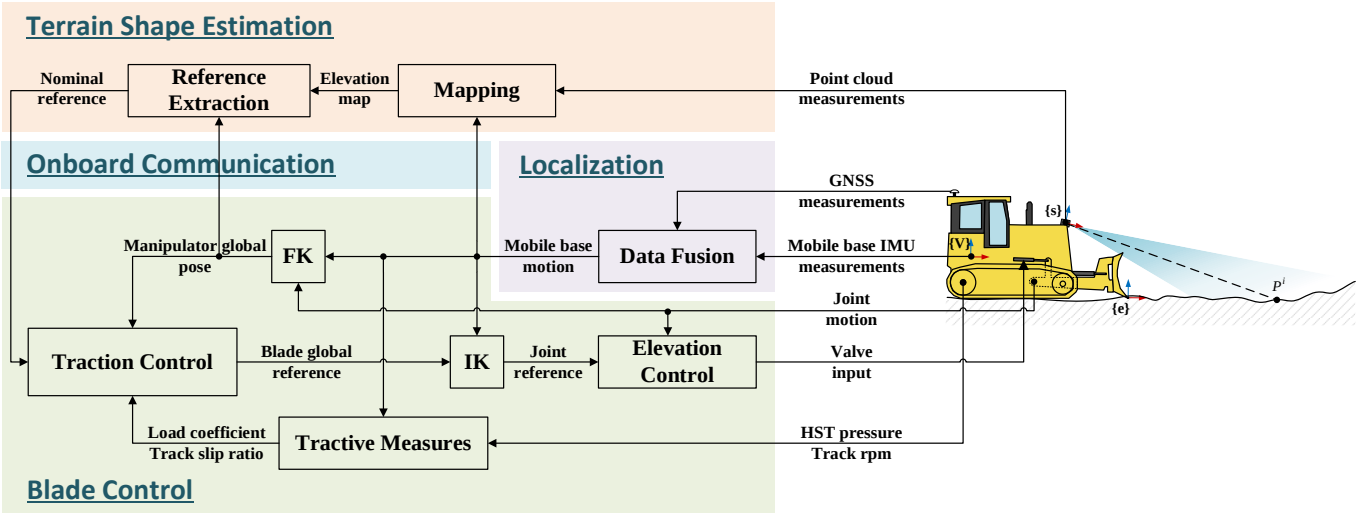

Fig. 2. General block diagram of the overall onboard solution with terrain shape estimation (Section III) and blade control (Section IV). Auxiliary components include the mobile base localization (Section III.A) and onboard communication between real-time control hardware and mapping hardware (discussed in Section V). The forward (FK) and inverse kinematics (IK) provide static and differential outputs.

The first objective is achieved by measuring the load experienced by the machine and controlling the blade elevation to maintain a desired load that indicates the amount of material pushed by the blade. The second objective is achieved by generating a smooth nominal path z_G based on the map of the environment and filtering the measured load value appropriately. The software modules and their interconnectivity are illustrated in Fig. 2. Each module is implemented using onboard hardware. The terrain shape estimation module consists of a mapping algorithm and a nominal reference generator. The blade control module includes an inner position control loop and an outer traction control loop. The localization output is used by many of the individual software blocks, making it an important part of the solution.

III. Terrain Shape Estimation

This section describes the terrain shape estimation module illustrated in Fig. 2. To obtain the terrain shape in suitable format for a control system, we propose a procedure as follows: (i) localize the visual sensor frame ***s*** in the reference frame ***I*** (Section III.A), (ii) generate and update an elevation map of the terrain using visual sensor measurements P^i transformed from frame ***s*** to frame ***I*** using the localization output (Section III.B), and (iii) compute a well-behaved reference from the elevation map to express the ground shape with continuous gradients to be used as an input to a blade controller (Section III.C).

A. Localization

The 6-dof pose of the mobile base frame ***V*** (see Fig. 1) is estimated by combining real-time kinematic global navigation satellite system (RTK-GNSS) and inertial measurement unit (IMU) data using an extended Kalman filter (EKF) based on [19]. The data fusion algorithm combines position and yaw data from a GNSS receiver with antennas installed on the cabin roof, and inertial data from a 3-axis IMU installed on the mobile base. To localize the sensor frame ***s***, the local transformation from ***V*** to ***s*** was used after localizing frame ***V***. The 16-element filter state is

$$\hat{x} = \begin{bmatrix} \hat{q}^T & \hat{b}_g^T & \hat{p}^T & \hat{v}^T & \hat{b}_a^T \end{bmatrix}^T, \quad (1)$$

where $\hat{q}$ is the estimated quaternion, $\hat{b}_g$ includes the gyroscope biases along each axis, $\hat{p}$ the estimated positions in the global frame ***I***, $\hat{v}$ the estimated velocities in frame ***I***, and $\hat{b}_a$ the 3-axis accelerometer biases. The transformation from the IMU location (frame ***V*** of Fig. 1) to the GNSS antenna is considered. The localization uses nonholonomic constraints to include knowledge of the vehicle dynamics to the filter equations [19] [20].

To account for external acceleration caused by soil interactions, the filter process noise covariance matrix (depicting IMU sensor noise) is adjusted online. Adapting methods for Kalman filters were considered in more detail in e.g., [21] and [22]. In this paper we update the process noise covariance as

$$U_k = A_k U, \quad (2)$$

where U is the nominal process noise covariance matrix, and the diagonal adaptation matrix A_k is computed for the accelerometer noise variance parameters a_{ij} as

$$a_{ij} = \begin{cases} 1 + k_{adapt}(\hat{a}_{ext} - a_0), & \hat{a}_{ext} > a_0 \\ 1, & otherwise. \end{cases} \quad (3)$$

Here, $k_{adapt} > 0$ is an adaptation gain; a_0 is an external acceleration threshold value; and $\hat{a}_{ext}$ is computed as

$$\hat{a}_{ext} = \frac{1}{L}\sum_{k=1}^{L} |\Delta a_k|, \quad \Delta a_k = \|a_k\| - \|g\|, \quad (4)$$

where a_k is a vector of accelerometer measurements at epoch k, and g is the vector of gravity. Other diagonal elements of A_k are set to 1. This choice has the filter rely more heavily on gyroscope and GNSS data during dynamic motion. The gain k_{adapt} was experimentally tuned for desired performance.

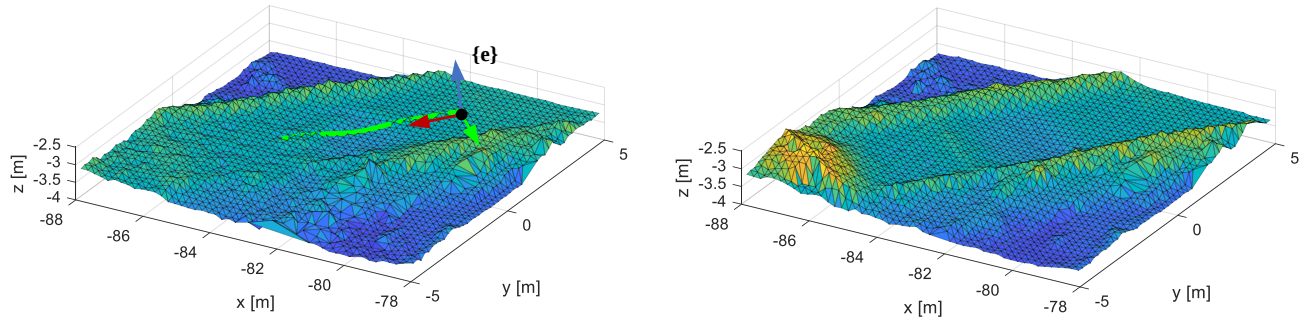

Fig. 3. Mapping performance and nominal reference computation. *Left*: Part of the map ahead of the blade illustrated as a triangular mesh, and the nominal blade path (green) during excavation. *Right*: the same part of the map updated while reversing after excavation. The soil pile carried on the blade to the end of the excavating area is visible at the left in the rightmost image. The surface color indicates height.

B. *Elevation Mapping*

The worksite mapping is based on the methodology used in [10] and [11]. The method uses a visual sensor to generate an x-y grid of map cells with elevation and variance values. Each measured robot-relative point P^i is expressed in frame $\boldsymbol{I}$ using the latest estimate of the mobile base motion (1) and calibration data for frame $\boldsymbol{s}$. Each map cell is updated with an elevation value using a Bayesian update scheme that considers the sensor measurement and calibration uncertainty and excludes exceptionally high-variance points from the map update.

On the experimental platform, masts installed on the blade and the blade itself can be perceived by the lidar (Fig. 4). Due to the simple structure of the manipulator, the points depicting a part of the robot itself could be filtered out using a distance filter on the point cloud data. An outlier rejection scheme based on adjacent point comparison was also implemented to increase the mapping robustness. For updating the map after soil excavation, a forgetfulness scheme was implemented to increase the variance of map cells based on the elapsed time since the most recent update. This way, the most recent data points are given priority over older ones and the map is updated rapidly as the excavated terrain comes into the view of the lidar sensor. The map update after excavating the soil is illustrated in Fig. 3, where the updated map is obtained while reversing back to the start of previous excavation.

The map resolution was chosen as 0.2 m to compromise between accuracy and algorithm complexity. For bulldozer blade control, this level of detail is generally enough as the machine is not used to track very high-fidelity terrain profiles in the longitudinal direction and the blade is typically at least 10 times wider than the resolution selected here.

C. *Nominal Reference*

The discrete height map is not in a format suitable to be used as an input to a control system. Hence, a smooth C^1 continuous curve is fitted to the terrain data up to distance d_L ahead of the vehicle along its direction of motion. To consider irregularities in the terrain captured by the map, and to enforce smooth blade motion references, each point of the map selected for fitting is averaged based on N neighboring points along the direction of motion. Then, a cubic spline is fitted to pass through the selected points, obeying the equations

$$z_G(s) = \gamma_0 + \gamma_1 s + \gamma_2 s^2 + \gamma_3 s^3, \tag{5}$$

$$\frac{\partial z_G(s)}{\partial s} = \gamma_1 + 2\gamma_2 s + 3\gamma_3 s^2, \tag{6}$$

where s is the normalized path parameter, and $\gamma_{0\ldots3}$ are the cubic polynomial parameters. In this paper, s is defined as the distance from spline start coordinates x_0, y_0, as $s = \sqrt{(x_e - x_0)^2 + (y_e - y_0)^2}$. The curve is computed in the yaw direction of the machine, with the estimated x and y coordinates of the end-effector frame $\boldsymbol{e}$ indicating its start coordinates, as illustrated in Fig. 1. As the mobile base advances on the terrain, map cells are updated with more reliable data at a closer range. The reliability of a point in the map reduces the further away it is from the blade. Hence, the curve is updated as the machine advances on the terrain. Updates are executed at a constant time interval of 1 second, as the terrain or the map is not expected to change dramatically at close range. Each new curve is constrained at its end points to have the gradient and elevation of the previous curve at those points. Since only the elevation of the blade is controlled in this study, the terrain roll angle is not included in the reference. The cubic nominal reference is illustrated on the map in Fig. 3.

IV. Blade Control

Due to the different goals during subtasks (Section II), we divide blade control into separate loading and carrying controllers that are used based on the bulldozer subtask within a work cycle. Transition from loading to carrying is made when one of the following conditions is true:

- Measured filtered external load force F_L exceeds target load force
- Track slip exceeds threshold value s_0.

For control, we normalize the external load force by the machine weight, obtaining the load coefficient $c_L = F_L / W_v$. The computed track slip is low-pass filtered for control purposes.

The resulting elevation in the worksite coordinates for the blade to follow is computed by time integration of

$$\dot{z}_d = v_e \frac{\partial z_G(s)}{\partial s} + v_t \dot{z}_i, \tag{7}$$

where v_e is the Cartesian velocity of the end-effector, and s describes blade position along the path defined by (5); $\frac{\partial z_G(s)}{\partial s}$ is computed from (6); v_t is the vehicle longitudinal velocity computed from track rpm; and $\dot{z}_i$ is a velocity term from subtask i controller. Scaling $\dot{z}_i$ by v_t instead of v_e allows for near equal performance at varying travel velocities while not allowing $\dot{z}_i$ to tend to zero during large track slip (due to unexpected hardness of soil). Here, it is assumed that the tracks keep constant rpm during the work cycle. Computation of $\dot{z}_i$ varies based on the active subtask, as described in the following subsections. The global Cartesian reference for other directions than z is taken as their measured values (see [16] for details).

A. Loading

The loading velocity term is computed as

$$\dot{z}_{LOAD} = \alpha_L \Delta z, \tag{8}$$

where Δz is a constant digging velocity, and $\alpha_L \in [0, 1]$ is a velocity scaling factor. Velocity scaling is executed to enable a gradual start to the dig, and to realize the end of further digging when a threshold condition is met. The scaling factor is computed as

$$\alpha_L = \alpha_{\Delta p} \alpha_{c_t}, \tag{9a}$$

$$\alpha_{\Delta p} = \min\left(1, \frac{\|p_B - p_0\|}{\Delta p}\right), \tag{9b}$$

$$\alpha_{c_t} = \max\left(0, \min\left(1, \frac{c_{L0} - \hat{c}_L}{c_{L0} - c_{L1}}\right)\right), \tag{9c}$$

where p_0 is the starting position of the blade; Δp is the length of gradual start, where $\dot{z}_{LOAD}$ increases linearly from 0 to Δz; c_{L0} is the threshold value where $\dot{z}_{LOAD} = 0$; c_{L1} is the threshold where $\dot{z}_{LOAD}$ starts to reduce linearly as a function of filtered measured $\hat{c}_L$ (see Section IV.C for details). Function (9b) is active at start of loading to request a smooth lowering of the blade. Function (9c) is active when $\hat{c}_L$ approaches the desired c_{Ld} during loading. The blade is then not lowered further, as the accumulating soil pile will typically increase the load to c_{Ld}. If this is not the case, an additional distance threshold can be used.

B. Carrying

The carrying subtask control is implemented using a (normalized) force feedback control strategy. During the carrying subtask, the reference velocity is computed as

$$\dot{z}_{CARRY} = k_f f_\epsilon(\hat{c}_L - c_{Ld}) + k_s(\max(s_L, s_R) - s_0), \tag{10}$$

where k_f is a positive traction control gain; c_{Ld} is the desired load coefficient; k_s is a positive slip feedback gain; s_L and s_R are the left and right track slips, respectively; and s_0 is a maximum allowable slip value. The slip-related-term is only active when $\max(s_L, s_R) > s_0$ and $\max(\dot{s}_L, \dot{s}_R) > 0$. Function f_ϵ for an input signal u is computed as

$$f_\epsilon(u) = \frac{\text{sign}(u)u^2}{\text{sign}(u)u + \epsilon}. \tag{11}$$

The function gives smooth motion outputs near the origin [5]. We chose $\epsilon_+ < \epsilon_-$ based on the sign of u for fast reaction to $\hat{c}_L$ exceeding c_{Ld} and a more gradual tracking of c_{Ld} when $\hat{c}_L < c_{Ld}$. This choice reduces wavy patterns in z_d and enforces retaining traction, resulting in a reasonable compromise between the two control objectives.

C. Tractive Performance Measurements

The propulsion system includes a hydrostatic transmission (HST), from which the travel motor pressures can be measured. The external load force is estimated from the pressure signal as

$$F_L = i_G \varepsilon_m \frac{V_{g,m}}{d_t \pi} \Delta p_m \eta_{m,hm}, \tag{12}$$

where i_G is the gear ratio between the hydraulic motor and track wheel; ε_m is the relative displacement of the hydraulic motor, $V_{g,m}$ is its maximum displacement; d_t is the track wheel diameter; Δp_m is the pressure across the travel motor; and $\eta_{m,hm}$ is the hydromechanical efficiency of the motor. While (12) describes a steady state force, it has utility in controlling the blade, as the force is tracked with error tolerance described by (11), and it is filtered based on dynamic motion as described next.

The measured HST pressure experiences changes when the machine body pitches, steers, or accelerates. Therefore, we implemented an exponentially weighted moving-average filter to suppress these effects seen in (12). This way, the blade controller does not react to these temporary effects while retaining performance during steadier motion. The filter is given by $y(n) = (1 - \alpha)y(n - 1) + \alpha z(n)$, where the newest input $z(n)$ has the weight α and the past filtered values $y(n - 1)$ are weighted by $(1 - \alpha)$ [23]. The weight parameter α is manipulated online based on the measured motion. In this paper, a nominal value α_0 is assigned to the filter, and its value is decreased according to the measured values of the effects to be filtered. These values are pitch angular velocity $\dot{\varphi}$ and acceleration $\ddot{\varphi}$; difference between left and right track angular velocities $\Delta\omega = |\omega_{wL} - \omega_{wR}|$; and external acceleration a_{ext}. The filter parameter is computed as

$$\alpha = \kappa_{\dot{\varphi}} \kappa_{\ddot{\varphi}} \kappa_{\Delta\omega} \kappa_{a_{ext}} \alpha_0, \tag{13}$$

where κ_i is computed as

$$\kappa_i = \frac{u_{thr,i}}{\max(u_{thr,i}, |u_i|)}, \tag{14}$$

with $u_{thr,i}$ indicating a threshold value activating the reduction of α, and u_i denoting the measured value of the signal i.

The track slip ratio is computed as

$$s_i = \begin{cases} 1 - \dfrac{|v_i|}{r_w|\omega_{wi}|}, & |v_i| \le r_w|\omega_{wi}| \\ -1 + \dfrac{r_w|\omega_{wi}|}{|v_i|}, & |v_i| > r_w|\omega_{wi}|, \end{cases} \tag{15}$$

where i denotes left or right track, v_i is the track longitudinal velocity, r_w is the track wheel radius, and ω_w is the track wheel angular velocity. Each velocity v_i is computed from estimated machine velocity in (1) and bias-corrected gyroscope data using kinematics, while rpm sensors are used for obtaining ω_w.

Fig. 4. The experimental setup and sensors installed on the machine. Masts on the blade are not used in this study.

D. Elevation Control

The blade elevation controller to follow (7) has been described in [16]. The hydraulic cylinders are controlled with velocity feedforward and position feedback to follow the desired blade elevation in the worksite coordinate frame. Experimental results in [16] show a surface tracking root mean square error of less than 3 cm, which is accurate enough for traction control showcased in Section VI here. With the localization algorithm adaptation proposed here, the localization problems described in [16] were solved. The control scheme uses the desired Cartesian velocity reference of (7) and its integral and requires differential inverse kinematics used as described in [16].

V. Experimental Setup

The proposed solution was verified in an experimental setup, involving a commercial Shantui DH13K LGP bulldozer. No modifications were made to the original hydraulics. Sensors were installed onboard the machine as illustrated in Fig. 4. The terrain point cloud measurements were obtained with a Hokuyo YVT-35LX lidar [24] mounted on the engine bay. The localization used RTK-GNSS with antennas mounted on the cabin roof and an IMU mounted on the cabin. Lift joint motion (angle and angular rate) was computed using the cabin and blade IMU measurements. The elevation mapping was executed on an Nvidia Jetson located inside the cabin. The localization and control algorithms were implemented on a dSPACE MicroAutoBox running at a 5-millisecond sampling interval. The mapping hardware communicated with dSPACE using Ethernet.

The tests took place during winter in Finland, with the ground frozen. To test the system, a layer of loosened soil material was spread on top of the frozen soil to have 10-20 cm of manipulable soil. In many of the experiments, the blade could not follow the desired elevation due to contact with impenetrable soil. In this paper, we showcase results from experiments where this problem was not very pronounced, as the proposed system was not designed to handle such a scenario. Based on our experiments, the maximum steady-state load coefficient that could be achieved on the test site soil without track slip was below 0.7. The target load was selected with this in mind. The mobile base motion was manually operated by driving in a straight line with only minor steering maneuvers and the track rpm remaining nearly constant.

VI. Experimental Results

Fig. 5 illustrates blade control results on ground profile with minor gradient changes. The load coefficient was kept near its desired value, while the requested blade elevation contained small changes. The blade followed the shape of the nominal reference profile obtained from the generated map. The force controller generated a cut at the start (0-5m) and made small adjustments once the desired loading condition had been reached for the first time. During the experiment, two minor steering maneuvers were executed to keep the machine aligned with the spread soil. These maneuvers are highlighted in Fig. 5. The measured load increased during each maneuver but decreased after the maneuver was finished. The proposed filter filtered out these increases effectively, causing the requested blade elevation to not react to these effects. Track slip ratio remained low (less than 0.15) throughout the experiment, and a reasonable amount of material was carried on the blade (not documented by

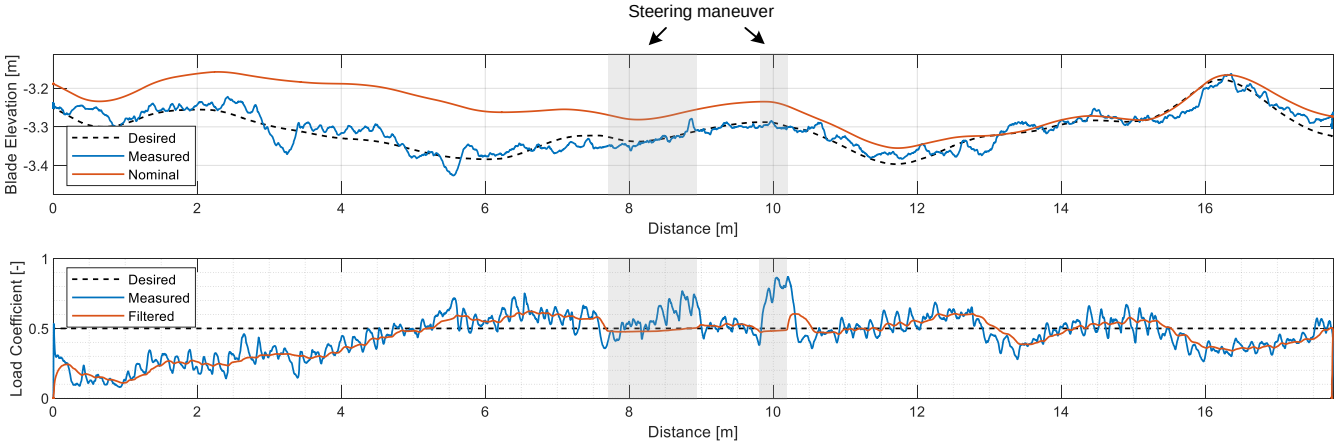

Fig. 5. Experimental results on ground with small gradient changes. The top figure illustrates the blade motion, while the bottom figure shows the estimated load coefficient and filtering behavior. The measured blade elevation is computed using forward kinematics, indicating the machine vibration and joint angle sensor noise. The machine traveled at approximately 0.45 m/s.

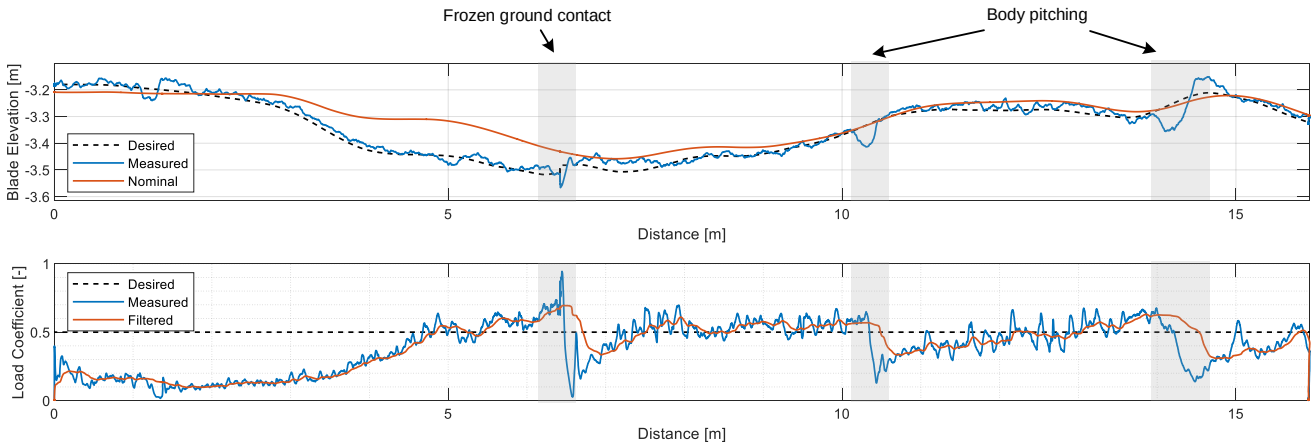

Fig. 6. Experimental results on ground with gradient changes as available at the test site. The machine traveled at approximately 0.35 m/s.

sensors). The trade-off between a smooth blade locus and external load tracking is seen in the errors in the latter. The desired load coefficient was gradually reached by maneuvering the blade smoothly.

Results on a surface with changes in the gradient are depicted in Fig. 6. In the experiment, the blade made contact with frozen soil, causing the tracks to start slipping, temporary causing full slip. By gradually lifting the blade, the machine regained desired mobility, which showcases the system performance in difficult conditions. The changes in the resulting ground profile gradient caused the mobile base to pitch, which is seen in the later parts of the experiment. This showcases the importance of smooth profiles on blade control accuracy with non-high-performance hydraulic valves. The external load force estimated from the measured HST circuit pressure shows changes due to this body motion. The proposed filter reduced blade reaction to these changes, making the requested blade elevation smooth in those parts. Again, the load coefficient tracking suffered temporarily, but was reached in a reasonable distance by gradually maneuvering the blade.

In both experiments shown here, the blade controller automatically generated a cut trace with initial filling of the blade followed by carrying of the accumulated soil material along the existing surface. The transition between filling and carrying was smooth, and the tractive performance was in an acceptable range throughout the experiments. Track speed was not reduced during operation as opposed to [5], as the blade reacted to terrain shape before it had a large effect on the load on the machine. Compared to the blade-only strategy in [5], the blade motion was much smoother. However, the proposed method was not tested on a worksite with such a large uphill. Contrary to [12], the terrain sensor was mounted on the mobile base, removing the need for a separate sensor system that may need to be relocated in the worksite as the work progresses.

VII. Conclusions and Future Work

This paper described a blade control approach to semi-autonomous earthmoving by heavy-duty bulldozers. The proposed solution produced a surface elevation profile to a blade position controller such that the load on the machine was controlled to a desired value while maneuvering the blade smoothly. The approaching terrain shape was estimated using onboard sensors and included in the control loop to prevent large load variations caused by terrain irregularities, hindering solutions operating without terrain shape information. The controller had two contradicting goals: (i) excavate a full blade of material: i.e., realize the desired load on the machine, and (ii) generate a smooth blade locus for the tracks to travel on. The first goal was met by normalized load force feedback control to set a world frame reference trajectory to a blade position controller. The second goal was achieved by a filtering method for restricting the desired blade motion, and by generating a smooth nominal blade path from the discrete, online generated worksite map.

The solution was tested in an experimental setup including a commercial bulldozer with no modifications to its original hydraulic system, and a retrofitted set of sensors for localizing the machine, querying the environment using a lidar, and controlling the manipulator according to measured tractive performance and the shape of the approaching terrain. The experimental tests were carried out in difficult conditions during winter in Finland. The results showed that the desired blade locus followed the estimated terrain shape in a smooth manner, while the desired load on the machine was maintained and asymptotically reached. The proposed filtering scheme had the blade react during steady motion, further enforcing smooth requested blade loci. In the challenging test conditions, the results were promising, and showcase the potential of the concept. However, some of the experiments failed due to contact with impenetrable frozen soil and were omitted from the paper as exceptional scenarios.

Industrial applicability of the proposed solution is also promising, as the required sensing and computing hardware was installed on a commercial machine without modifications to its original hydraulic components. While the efforts needed to achieve a commercial product are vast, the results of this paper show that many of the individual problems related to the use case can be solved. While the type of lidar used in this study is susceptible to damage from extreme vibration and acceleration, a solid-state lidar sensor could be robust enough to not be at risk of breaking in such conditions.

The proposed solution needs to be tested in conditions without frozen soil, as this was not possible at the test site at the time of experimental testing. The machine could then be operated at higher travel velocity without risking track wear during sudden blade contact with unmanipulable soil. In the future, the earthmoving efficiency can be further increased by online optimizing the desired machine load based on identified soil characteristics and desired operation metrics. While not considered here, the shape of the worksite design surface can be included in the blade reference in a straightforward way. When possible, the ground surface prior to soil excavation should contain larger gradients and changes to test the proposed method in different conditions.

ACKNOWLEDGMENT

This work was funded by the Doctoral School of Industry Innovations (DSII) of Tampere University.

REFERENCES

[1] J. Harada and E. Ishibashi, "ICT Bulldozer D61EXi/PXi-24, Automatic Dozing Control Improved Technology," *Komatsu Technical Report,* vol. 64, no. 171, 2018.

[2] P. Osinenko and S. Streif, "Optimal traction control for heavy-duty vehicles," *Control Engineering Practice,* vol. 69, pp. 99-111, 2017.

[3] P. K. Pranav, V. K. Tewari, K. P. Pandey and K. R. Jha, "Automatic wheel slip control system in field operations for 2WD tractors," *Computers and Electronics in Agriculture,* vol. 84, pp. 1-6, 2012.

[4] K. Hayashi, K. Shimada, E. Ishibashi, K. Okamoto and Y. Yonezawa, "Development of D61EXi/PXi-23 Bulldozer with automatic control system of work equipment," *Komatsu Technical Report,* vol. 59, no. 166, 2013.

[5] T. Mononen, J. Mattila and M. M. Aref, "High-level controller for high productivity earthmoving by tracked bulldozers," in *2020 ASME Symposium on Fluid Power and Motion Control (FPMC)*, Virtual, 2020.

[6] D. Jud, P. Leemann, S. Kerscher and M. Hutter, "Autonomous Free-Form Trenching Using a Walking Excavator," *IEEE Robotics and Automation Letters,* vol. 4, no. 4, pp. 3208-3215, October 2019.

[7] M. Hirayama, J. Guivant, J. Katupitiya and M. Whitty, "Path planning for autonomous bulldozers," *Mechatronics,* vol. 58, pp. 20-38, 2019.

[8] E. Halbach, *High-Level Job Planning for Automated Earthmoving*, Helsinki: Dissertations, Aalto University, 2016.

[9] H. Cannon, Extended earthmoving with an autonomous excavator, The Robot. Inst., Carneige Mellon Univ., Tech. Rep. CMU-RI-TR-99-10, 1999.

[10] A. Kolu, M. Lauri, M. Hyvönen, R. Ghabcheloo and K. Huhtala, "A mapping method tolerant to calibration and localization errors based on tilting 2D laser scanner," *2015 European Control Conference (ECC),* pp. 2348-2353, 2015.

[11] A. Kleiner and C. Dornhege, "Real-time localization and elevation mapping within urban search and rescue scenarios," *Journal of Field Robotics,* vol. 24, pp. 723-745, 2007.

[12] S. G. Olsen and G. M. Bone, "Model-Based Control of Three Degrees of Freedom Robotic Bulldozing," *ASME. J. Dyn. Sys., Meas., Control.,* vol. 136, no. 2, March 2014.

[13] S. G. Olsen and G. M. Bone, "Development of a Hybrid Dynamic Model and Experimental Identification of Robotic Bulldozing," *ASME. J. Dyn. Sys., Meas., Control,* vol. 135, no. 2, March 2013.

[14] S.-H. Kim, Y.-S. Lee, D.-I. Sun, S.-K. Lee, B.-H. Yu, S.-H. Jang, W. Kim and C.-S. Han, "Development of bulldozer sensor system for estimating the position of blade cutting edge," *Automation in Construction,* vol. 106, 2019.

[15] Y.-S. Lee, S.-H. Kim, J. Seo, J. Han and C.-S. Han, "Blade control in Cartesian space for leveling work by bulldozer," *Automation in Construction,* vol. 118, 2020.

[16] T. Mononen, J. Mattila and A. Kolu, "Blade Control for Surface Profile Tracking by Heavy-Duty Bulldozers," in *ASME/Bath Symposium on Fluid Power and Motion Control (FPMC)*, Virtual, Online, 2021.

[17] "Grade Control for Dozers," Trimble Inc., [Online]. Available: https://construction.trimble.com/products-and-solutions/grade-control-dozers. [Accessed 26 April 2021].

[18] T. D'Adamo, T. Phillips and P. McAree, "Registration of three-dimensional scanning LiDAR sensors: An evaluation of model-based and model-free methods," *J Field Robotics,* vol. 35, no. 7, p. 1182– 1200, 2018.

[19] R. Munguía, "A GPS-Aided Inertial Navigation System in Direct Configuration," *Journal of applied research and technology,* vol. 12, no. 4, pp. 803-814, 2014.

[20] G. Dissanayake, S. Sukkarieh, E. Nebot and H. Durrant-Whyte, "The aiding of a low-cost strapdown inertial measurement unit using vehicle model constraints for land vehicle applications," *IEEE Transactions on Robotics and Automation,* vol. 17, no. 5, pp. 731-747, Oct. 2001.

[21] Á. Odry, R. Fullér, I. J. Rudas and P. Odry, "Kalman filter for mobile-robot attitude estimation: Novel optimized and adaptive solutions," *Mechanical Systems and Signal Processing,* vol. 110, pp. 569-589, 2018.

[22] A. H. Mohamed and K. P. Schwarz, "Adaptive Kalman Filtering for INS/GPS," *Journal of Geodesy,* vol. 73, pp. 193-203, 1999.

[23] L. Hulttinen, J. Koivumäki and J. Mattila, "Parameter identification for improved performance of model-based control of hydraulic manipulators," in *2019 IEEE International Conference on Cybernetics and Intelligent Systems (CIS) and IEEE Conference on Robotics, Automation and Mechatronics (RAM) (pp. 124-129)*, Bangkok, 2019.

[24] Hokuyo Automatic Co., "Distance Data Output/YVT-35LX," 2014. [Online]. Available: https://www.hokuyo-aut.jp/search/single.php?serial=224. [Accessed 4 January 2022].